EXPERIMENTAL INVESTIGATION OF SUBMERGED HORIZONTAL AIR–STEAM MIXTURE JETS INTO STAGNANT WATER

YAISEL CORDOVA[1,2], YAGO RIVERA[1], DAVID BLANCO[1], CÉSAR BERNA[1], JOSÉ LUIS MUÑOZ-COBO[1] & ALBERTO ESCRIVÁ[1]
[1]Instituto de Ingeniería Energética, Universitat Politècnica de València, Spain
[2]Instituto Superior de Tecnologías y Ciencias Aplicadas, Cuba

ABSTRACT

Direct discharge of a steam into pools with subcooled water is a very efficient way to condense steam. Therefore, steam discharges have been widely applied in the industry because they allow rapid condensation of steam by offering high heat transfer and mass exchange capacity. Many experiments of submerged jets of pure steam and non-condensable gases in pools have been carried out over the last few decades, providing much information of interest, but more studies continue to obtain a wider range of information. In particular, the study of non-condensable gases/steam mixtures is of great interest for the chemical, energy and nuclear industry. Therefore, the present study aims to investigate the jet behavior through a series of experiments of air/steam mixtures discharged in a pool with stagnant water. Several tests have been performed by varying parameters, such as the nozzles diameters, mixing percentages, pressures and flow rates. In the current research, the jet behavior is investigated through direct visualization techniques by using a high-speed camera and image processing methods. The images of the jet discharge in the pool have been recorded to determine the interface between the gas mixture and the liquid. To carry out image processing, a MATLAB subroutine consisting of several steps was implemented. Experimental results showed that the nozzle diameter and the percentage of mixing play a significant role in the jet interface and jet pinch-off unsteadiness. The jet penetration length also was strongly influenced by the nozzle diameter and the mixing percentage.
Keywords: non-condensable gas, steam, direct contact condensation, jets, two-phase flow, digital image processing.

1 INTRODUCTION

It is of great interest to the nuclear industry to know and understand the steam condensation in presence of non-condensable gases from the point of view of passive safety of nuclear reactor. In a postulated loss-of-coolant accident (LOCA) of a boiling water reactor (BWR), the suppression pool system (SP) is very important, because it can mitigate the threats of containment over-pressurization and release of fission products. During the initial blowdown, after cleaning the vents, non-condensable gases (air) and steam are discharged into the SP. The concentration of non-condensable gases decreases from 100% to less than 10% and then there is a longer period of steam injection [1].

There are currently several experimental studies on flow behavior in suppression pools, but most have been conducted with pure air or steam discharges. Discharges of mixtures of steam and non-condensable gases have not been studied in such depth due to their complexity since the presence of non-condensable gases considerably affects the condensation of a steam jet.

Kerney et al. [2] obtained a model for predicting the steam plume length considering a constant Stanton number, based on the relationship between the heat transferred to a fluid and its heat capacity. A lot of previous works [3]–[6] have obtained experimental correlations for steam plume length assuming the work presented by Kerney et al [2]. Harby et al. [7], [8] propose that depending on the relative importance of the inertial and buoyancy force, the jet

WIT Transactions on Engineering Sciences, Vol 128, © 2020 WIT Press
www.witpress.com, ISSN 1743-3533 (on-line)
doi:10.2495/AFM200091

flow along the downstream distance can be divided into momentum jet regime within a length from the nozzle exit and buoyant jet regime within a length measured from the end section of the momentum region. Chong et al. [9] suggest a theoretical model to predict and compare the steam jet lengths of different structural nozzles based on the expansion and compression waves theory. Many researchers [7], [10]–[14] have developed correlations for non-dimensional gas penetration length based on term of modified Froude number. Li et al. [15] develop a model where they propose that the gas mixture jet penetration length increases when increasing the inlet pressure and decreases when increasing the air fraction. The main Computational Fluid Dynamics (CFD) researches on the jet behavior is on steam jets. Zhou et al. [16] used a thermal equilibrium phase change model into Fluent as a User-Defined Function to model the DCC process. Multiphase Volume of Fluid (VOF) model is used in Shukla et al. [17] to track the interface and standard k-ϵ model was adopted for modeling the turbulence.

The experiments that will be carried out will allow us to expand the scarce database of steam discharges with non-condensable gases currently available. This will allow the community of users and developers of CFD codes can use them, validate and implement improvements to these codes.

2 EXPERIMENTAL FACILITY AND METHODS

2.1 Experimental facility

The facility performs a mixture of steam and air injection in a rectangular-based pool with subcooled water, as shown in Fig. 1. The water used during the execution of the experiments is previously purified by means of a reverse osmosis system, in order to eliminate possible impurities and limescale dissolved. The water pool has the dimensions (length x width x height) 1500 mm x 500 mm x 600 mm and all its walls are transparent and are made of glass to enable optical flow measurements.

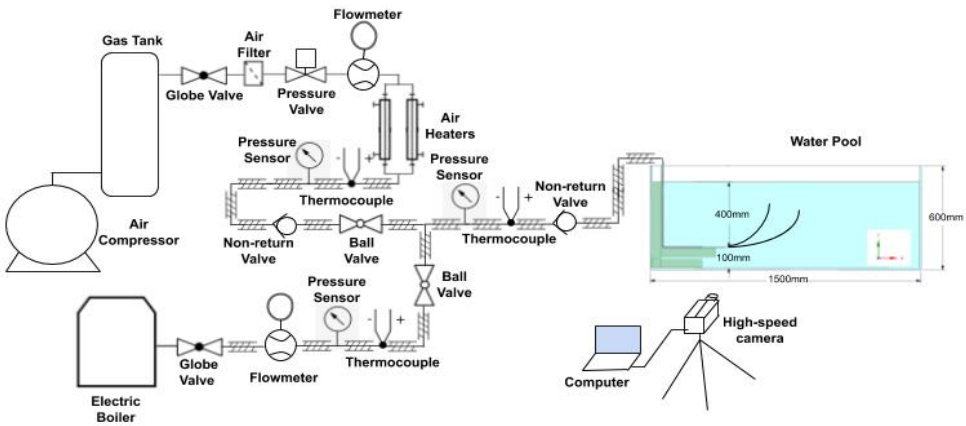

Figure 1: Schematic diagram of the experimental facility.

A water level of 500 mm is maintained in the horizontal jet experiments. Consequently, the rest of the height (100 mm) of the water pool is considered as free surface. Two interchangeable stainless steel nozzles of different internal diameters (5 mm, 6 mm) are used

for the injection, with the same length of 130 mm. The internal diameter of nozzles was chosen because it is the range of nozzle diameter used by many authors [7], [8], [18], [19]. These are located at a height of 400 mm below the water level and 100 mm from the pool bottom.

The injection of the pressurized air is achieved by means of a screw air compressor with a volume of 500 L, whose maximum operating pressure is 11 bar. Following the compressor is a gas tank (boiler) of 100 L in order to stabilize the air conditions prior to injection. The air flow is regulated by means of a globe valve and a precision valve. Afterwards it is measured with a flowmeter with an operating range of 50–500 l/min and a maximum pressure of 7.5 bar. In order to avoid steam condensation when mixing the air with the steam, it is necessary to heat the air, so the installations has two parallel air heaters FLUENT of 120 V and 500 W. The temperature control is carried out separately for each heater by means of a close-loop PID control system and with a DIN-a-mite power module, which allows the analogical control of the power. A thermocouple type "K" (± 0.1°C accuracy) is used to measure the process output temperature, which will be the set point.

An electric steam boiler is used to produce saturated steam. Its maximum operating pressure is 6.5 bar. A Krohne flowmeter with an operating range of 50–400 l/min is used to measure the steam volumetric flow. Downstream of the flowmeter is a pressure sensor and a thermocouple to monitor the pressure and temperature at which mixing takes place. After the mixing zone, a pressure and a temperature sensor are located to know the mixing parameters at the nozzle outlet. The hoses are made of a flexible material that supports temperatures up to 232°C and a pressure of 18 bar. They are thermally insulated to avoid losses.

The pressure, temperature and flow sensors are connected to a National-Instruments data acquisition system (Model 6259 16-bit) operated by Labview Software to monitor and control data acquisition. These will be used for further processing of the results.

A LED light panel with dimensions 1150 mm x 250 mm was placed at the back of the pool as a backlight in order to obtain clear images. The jet behavior is recorded by a 10 bit high-speed camera (PCO.1200 hs), with an exposure time range of 50 ns to 5 s, a shooting frequency of 636 frames per second (fps). The outside diameter of the nozzle was used as a length reference frame in the subsequent digital image processing (see Fig. 2).

Figure 2: Experimental facility.

2.2 Experimental initial conditions

This phase involves a series of experiments with air–steam mixtures that are discharged through a nozzle into a pool of initially stagnant water. The following quantities will be varied: volumetric flow injected into the pool, diameter of the injection nozzle and pressure at which the injection takes place (see Table 1).

Table 1: Summary of experimental initial conditions.

Nozzle diameter (mm)	Mixture velocity (m/s)	Air volumetric fraction, W_a
5	125, 175, 225	0.25, 0.5, 0.75, 1
6	125, 175, 225	0.25, 0.5, 0.75, 1

2.3 Image analysis method

The penetration length and the interface between the gas and the liquid were measured with direct visualization technique using a high-speed camera (CCD). The images obtained were saved in tagged image file format (TIFF) for further processing. First, it is recorded a reference (background) video. This image was used to calibrate and determine the number of pixels per millimeter based on the outside diameter of the nozzle. Then, the recording of the jet experiment starts. This video had a resolution of 1024 x 1280 pixels; each millimeter corresponded to 4 pixels approximately. The maximum number of images depends on the resolution and exposure time selected on the camera settings software. For this study, the maximum number that the camera can take before filling the RAM memory is 817.

To process these images, a multi-step routine is implemented in MATLAB. The original image was cropped to remove the part that was not important in the study (see Fig. 3(a)). Then, the "imbinarize" function is used to create a binary image from 2-D grayscale image using the specified threshold method (see Fig. 3(b)). Next, other function performs median filtering of the 2-D binary image where each output pixel contains the median value in the neighborhood around the corresponding pixel in the input image (see Fig. 3(c)). Because there are areas of the gas jet composed of several shades is applied a function for fills the holes in the input binary image. In this syntax, a hole is a set of background pixels that cannot be reached by filling in the background from the edge of the image (see Fig. 3(d)). Afterwards, the adjustment (morphological) operation is applied to remove small bubbles

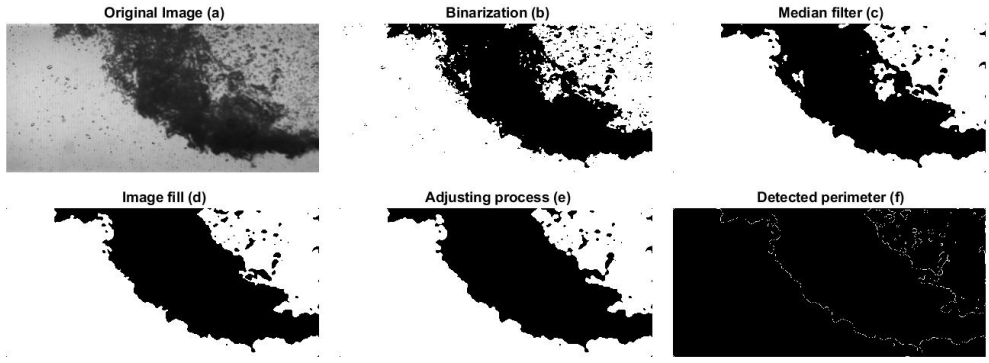

Figure 3: Steps used in the routine implemented in MATLAB to detect the jet boundary.

from the image, for these two functions are used; the first erodes the binary image and the second dilates the binary image, these functions use a disk-shaped structuring element with a radius $r = 6$ (see Fig. 3(e)). Finally, a function that returns a binary image that contains only the perimeter pixels of objects in the input image. A pixel is part of the perimeter if it is nonzero and it is connected to at least one zero-valued pixel (see Fig. 3(f)).

The jet pinch-off phenomenon refers to the state in which the jet is no longer continuous form the nozzle to the free surface. To calculate the position where the jet breaks, the jet perimeter (interface) is linearized, which means that for each x-coordinate position only one radial interface position (y-coordinate) is allowed.

The jet penetration length is defined as the length from the nozzle outlet to the intersection between the outer boundary of the jet and the axis of the nozzle. The average jet penetration length ($L_{m,b}$) is calculated by measuring 817 continuous images and taking an arithmetic mean value. The standard deviation (σ) is used to describe the dispersion of the average jet penetration length

$$L_{m,b} = \frac{1}{817} \sum_{i=1}^{817} L_{m,b}(i), \tag{1}$$

$$\sigma = \sqrt{\frac{1}{817-1} \sum_{i=1}^{817} (L_{m,b}(i) - L_{m,b})^2}. \tag{2}$$

The results of the processed images in MATLAB were obtained using the summation method, in which each processed image was added to the last one, resulting in an image with varying spatial intensity.

3 EXPERIMENTAL RESULTS AND DISCUSSION

In the present study, two nozzles were used to study the behavior of the discharge of air–steam mixture into pools with subcooled water. The air fraction (W_a) varied from 0.25 to 1 approximately for mixture velocity (u_m) of 125 m/s, 175 m/s and 225 m/s. Table 2 shows the results obtained for all experimental initial conditions studied. The dimensionless numbers, such as Reynolds and Froude number are calculated based on the parameters at nozzle outlet. The pressure values are absolute, where P_m is the jet pressure at mixture pressure sensor upstream of the injector. T_m is the mixture temperature measured by the thermocouple upstream of the injector. The air temperature was always kept above the steam temperature to avoid condensation (see Table 2).

The air fraction in some cases is not exactly the value predicted above because it is extremely dependent on the steam fraction. These values are obtained by data acquisition from the air and steam flowmeters and then the percentage that each one represents.

The jet zone where inertia force dominates can be called jet-dominated and the jet zone where buoyancy force dominates can be called plume-dominated. In the jet-dominated zone the strength of the jet is related to value of its Froude number. As previously stated, many authors give the momentum jet length as a function of the Froude number

$$Fr = \frac{u_m}{\sqrt{g(\Delta\rho/\rho_m)d}}, \tag{3}$$

where, $\Delta\rho$ is the subtraction of water density (ρ_w) and mixture density (ρ_m), d is the inner diameter of nozzle. The mixture density is considered as a weighted average, calculated from the total mass and total volume flow rate. This mass is obtained from the volume flow rate of each fluid and the specific density, considering a homogeneous mixture.

Table 2: Experimental test matrix and jet initial boundary conditions.

d (mm)	W_a	Fr	Mach	P_m (Pa x 10^5)	ρ_m (kg/m^3)	T_m (K)	$\dot{m}$ (x 10^{-3} kg/s)	u_m (m/s)	Re (x 10^5)
5	1	23.19	0.34	1.59	1.60	385.95	4.00	127.3	0.46
5	0.733	20.58	0.31	1.51	1.26	379.75	3.15	127.3	0.43
5	0.5	17.04	0.27	1.37	0.99	380.05	2.31	118.8	0.36
5	0.267	17.05	0.28	1.34	0.86	380.05	2.16	127.3	0.38
5	1	31.69	0.47	1.59	1.60	383.15	5.47	174	0.63
5	0.732	28.86	0.43	1.59	1.33	385.95	4.53	174	0.63
5	0.5	26.29	0.39	1.59	1.16	385.95	3.86	169.8	0.60
5	0.262	24.55	0.39	1.43	0.91	389.55	3.20	178.3	0.56
5	1	42	0.62	1.57	1.68	359.09	7.40	224.9	0.87
5	0.75	45	0.54	2.43	2.04	385.45	8.82	220.7	1.20
5	0.5	41	0.49	2.43	1.76	388.15	7.73	212.2	1.14
5	0.245	40	0.49	2.32	1.49	395.05	6.59	224.9	1.16
6	1	18.4	0.34	1.20	1.28	370.43	4.48	123.8	0.43
6	0.762	18.02	0.31	1.37	1.23	374.25	4.29	123.8	0.49
6	0.5	15.93	0.29	1.27	0.96	375.65	3.35	123.8	0.44
6	0.238	14.36	0.27	1.20	0.78	377.75	2.73	123.8	0.41
6	1	27.52	0.49	1.33	1.45	371.31	7.31	173.9	0.68
6	0.746	26.02	0.44	1.50	1.30	380.75	6.37	173.9	0.72
6	0.5	23.62	0.41	1.39	1.03	381.65	5.16	176.8	0.67
6	0.254	20.78	0.38	1.27	0.83	381.85	4.06	173.9	0.59
6	1	38.32	0.63	1.51	1.69	372.15	10.72	224	1.03
6	0.75	37.37	0.57	1.80	1.61	374.65	10.20	224	1.17
6	0.5	32.66	0.53	1.61	1.23	378.85	7.79	224	1.03
6	0.25	31.61	0.50	1.70	1.15	385.15	7.30	224	1.07

3.1 The surface undulation

The surface undulation is produced because the jet discharge produces three kinds of perturbation in the initial contained in the pool. These perturbations are of three types the first one is that the jet discharged into the liquid expands as it penetrates in the pool and this expansion obviously produces a change in the free surface of the pool that changes its profile and height. Second because the contour of the jet is oscillating these oscillations are transmitted through the liquid to the free surface. And third the non-condensing gas that moves upward to the surface also perturbate the surface. So, the surface is perturbated and oscillates, but the jet in not re-entering. These oscillations are seen clearly in Fig. 2.

3.2 Momentum gas jet length

Fig. 4 shows the experimental results for horizontal buoyant jet in stagnant water at different air fraction for nozzle diameter of 5 mm. The contour colors indicate how many times in the images a certain place in the field of vision is occupied by the mixture of air and steam, this was obtained by a summation method in MATLAB.

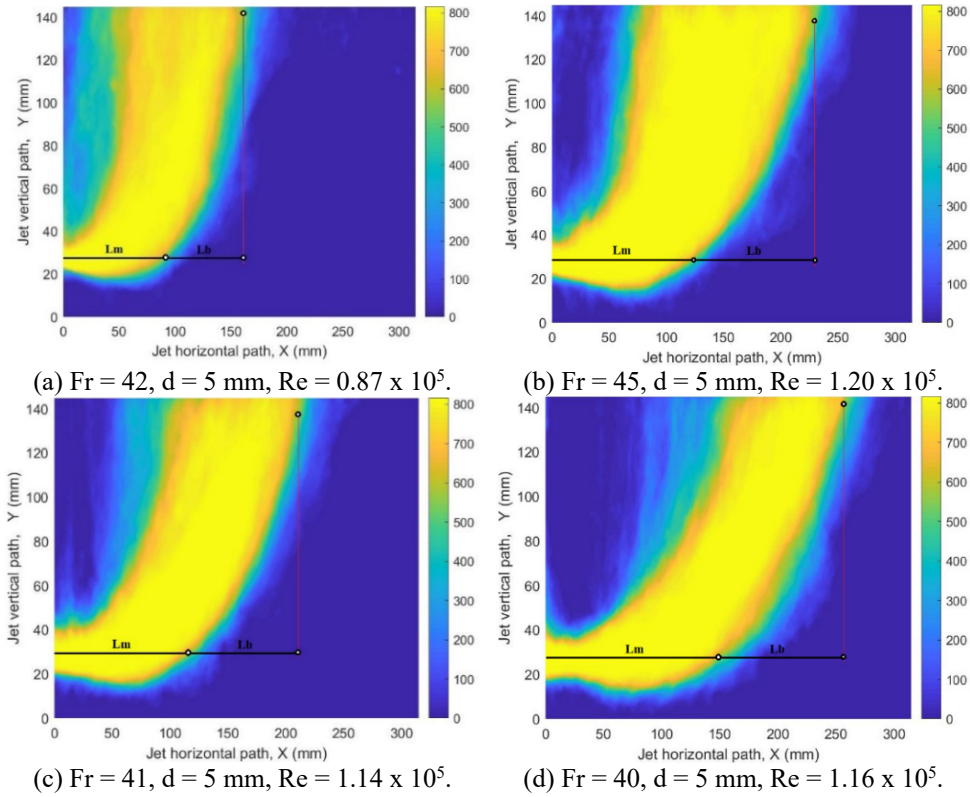

(a) Fr = 42, d = 5 mm, Re = 0.87 x 10^5. (b) Fr = 45, d = 5 mm, Re = 1.20 x 10^5.

(c) Fr = 41, d = 5 mm, Re = 1.14 x 10^5. (d) Fr = 40, d = 5 mm, Re = 1.16 x 10^5.

Figure 4: Experimental results for horizontal buoyant jets in stagnant water. (a) Wa = 1; (b) Wa = 0.75; (c) Wa = 0.5; and (d) Wa = 0.25.

In Fig. 4(a) there is only air that is why the momentum jet length is so small, because the buoyancy forces make the jet go up faster. In Fig. 4(b)–4(d), as the steam fraction increases, it makes the momentum force greater than the buoyancy force, and therefore the momentum jet length rises and when the air fraction is 0.25 the greatest momentum jet length is obtained. Furthermore, an obvious difference can be observed between the two jets when the air fraction is 0.75 and 0.5, especially marked because at 0.75 the jet occupies a larger space for a large set of images percentage.

3.3 The influence of air fraction on the momentum and buoyancy length

Fig. 5(a) and 5(b) show the influence of air fraction on the momentum length (L_m) at the two nozzles for different velocities. The momentum length for higher velocity and air fraction of

0.25 is the greatest, for both the 5 mm and the 6 mm nozzle. For air fraction of 0.5 the momentum length decreases and for 0.75 the momentum length increases again, this we believe may be caused by the three phenomena present, the inertia, the buoyancy force and the steam condensation, and depending on the air fraction will influence one phenomenon more than the other. Finally, when the air fraction is 1, in other words, there is only air, the momentum length decreases again.

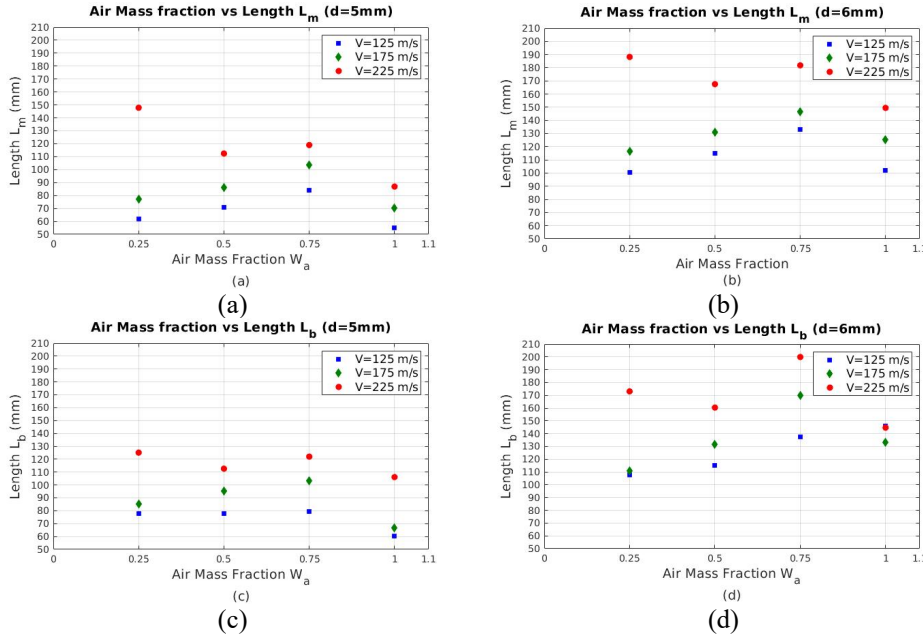

Figure 5: The influence of air fraction on momentum and buoyancy length. (a) L_m (5 mm); (b) L_m (6 mm); (c) L_b (5 mm); and (d) L_b (6 mm).

For the velocities 125 m/s and 175 m/s, the momentum length increases until the air fraction is 0.75 and then decreases. This is because, for these velocities, the air fraction is so small that in the balance between buoyancy force and steam condensation, steam condensation predominates, causing the momentum length to increase until the air fraction is 0.75.

The lift force is an important force for bubbles moving in fluid with a velocity gradient or a velocity rotational field. This is not the present case for a jet discharge. The virtual mass force it is important for bubbles moving through a carrier fluid with density much higher than the density of the gas bubbles. The bubbles in their motion accelerate the surrounding carrier fluid and displace it. The effect is that to apply the newton law to the bubble's motion we must consider that the bubbles have a higher mass that is called "virtual mass", this virtual mass is obtained adding to the bubble mass a term $0.5\ \rho_l\ V_b$. Where V_b is the bubble volume and ρ_l is the density of the liquid phase. This is not the case for the jet discharge into a pool.

There is some drag of small drops being removed at the interphase, by the interfacial stress forces acting on the interface between both fluids in the jets. These forces are normally considered in the modelling of jet discharges in pools (see Harby et al. [8]).

3.4 The influence of velocity on the momentum and buoyancy length

Fig. 6 shows the influence of velocity on the momentum length (L_m) at the two nozzles for different air fractions. The momentum length increases with the rise of velocity for the four air fractions, which is because by increasing the velocity and with it the Froude number, the transition point to the buoyancy-controlled regime moves further, downstream from the nozzle outlet, which is consistent with the analysis results. As shown in the Fig. 6(d), when only air is present the length increases following a linear function and the shortest momentum length is obtained. However, for an air fraction of 0.25 (see Fig. 6(a)), the longest length is observed for the velocity of 225 m/s, this could probably be explained because the increase in velocity brings about an increase in the steam percentage in the mixture and thus the steam condensation make the length longer.

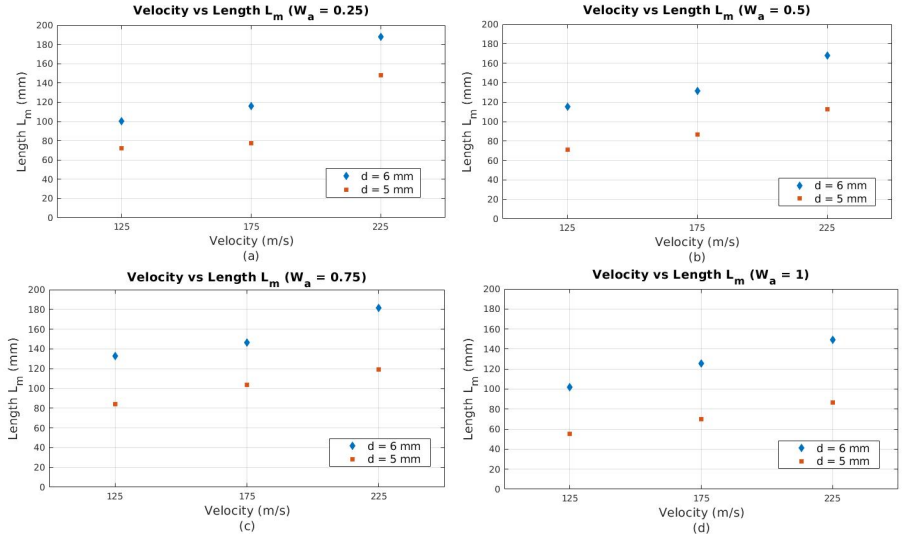

Figure 6: The influence of velocity on momentum length.

Fig. 7 shows the influence of velocity on the buoyancy length (L_b) at the two nozzles for different air fractions. The buoyancy length increases with the rise of velocity for the four air fractions, except for the case of velocity of 125 m/s and diameter of 6 mm. In Fig. 7(a)–7(c) can be observed that the existence of air will greatly reduce the heat transfer coefficient of the condensation and provide a buffering effect in the final stage of the steam bubble collapse. As shown in the Fig. 7(c), for air fraction of 0.75, the longest buoyancy length is obtained for the velocity of 225 m/s and nozzle diameter of 6 mm.

3.5 Correlations for predicting dimensionless length of momentum and buoyancy

The dimensionless momentum length is defined as the ratio of the momentum length (L_m) to the nozzle inner diameter (d), and the dimensionless buoyancy length is the same, but with buoyancy length (L_b). The fits were made using a MATLAB function, where some adjustment coefficients were also obtained.

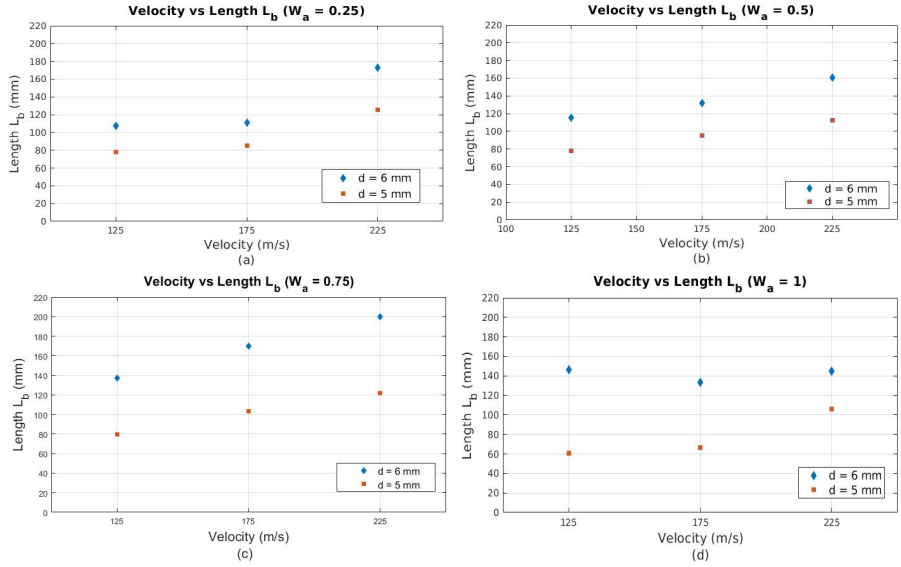

Figure 7: The influence of velocity on buoyancy length.

For dimensionless momentum length, the appropriate correlations is

$$\frac{L_m}{d} = 1.9103 \cdot 10^{-4} Re^{1.3482} Fr^{-1.0461}. \tag{4}$$

For dimensionless buoyancy length, the appropriate correlations is

$$\frac{L_b}{d} = 1.5821 \cdot 10^{-3} Re^{1.0976} Fr^{-0.831}. \tag{5}$$

The Reynolds number considered in this paper is a ratio of the inertial to the viscous forces of the fluid, while the Froude number is the ratio of the inertial force to the gravity field force. This means that in the correlations used in this paper we are considering the ratios of the main forces acting on the jet.

Where the Reynolds Re and Froude Fr numbers are expressed in terms of mixture parameters. The fitting of the proposed correlations with the obtained experimental results is shown in Fig. 8. As can be seen in the figure, the correlation fits quite well with the experimental results, obtaining a value for the Pearson product-moment correlation coefficient of $R^2 = 0.941$ for dimensionless momentum length and $R^2 = 0.835$ for dimensionless buoyancy length.

In these correlations, the relative influence of each term can be observed, with the Reynolds number having the higher weight because it is raised to a slightly higher exponent value. In addition, the Reynolds number is directly related to dimensionless length, as it is raised to a positive number. While that Froude number is inversely proportional by having a negative exponent. These dimensionless coefficients depend on the fluid properties, with air and steam proportions intervening here, which will mark the characteristics of the fluid.

In Fig. 8(a), it can be seen how the correlation for the length of the dimensionless momentum fits the experimental data remarkably well. About 55% of the data points are within the –5% to +5% error band. While almost all the remaining points are within the –20% to +20% error band, only one point is outside the band, but very close.

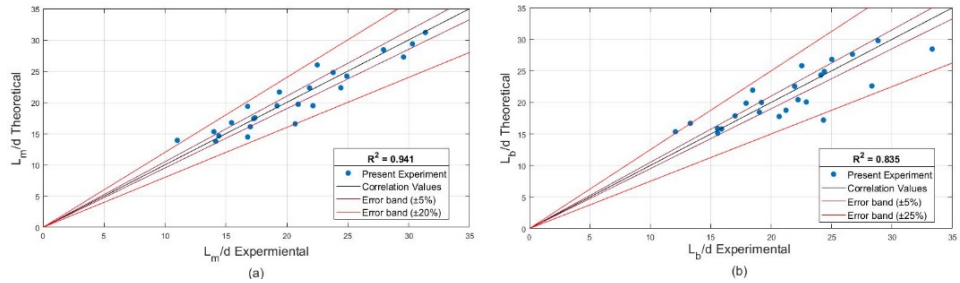

Figure 8: Comparison of the results obtained for dimensionless length correlation and the experimental results. (a) Momentum length; and (b) Buoyancy length.

Fig. 8(b) shows the comparison of the results obtained for the dimensionless buoyancy length correlation and the experimental results. In this case, more than 45% of the points are within the –5% to +5% error band. While almost all the remaining points are within the –25% to +25% error band, as in the case of the previous correlation, there is point that is outside this band. This point corresponds to the velocity of 125 m/s and the air fraction of 1, Fig. 7(d). The point characterizes the velocity of 125 m/s and the diameter of 6 mm does not follow the same distribution present in the in the other results obtained that characterized the increase in length with velocity. Seeing that it could be an error when carrying out the experiments, it is proposed as a future work to repeat the experiment for this configuration.

4 CONCLUSIONS

The behavior of the air–steam mixture jet discharged into stagnant water was investigated for two nozzle diameters and several air fractions in the mixture using a high velocity camera. The main conclusions obtained in this work are:

1. The results of the processed images in MATLAB were obtained using the summation method, in which each processed image was added to the last, resulting in an image with varying spatial intensity.
2. The momentum length increases with the rise of the initial jet velocity for four air fractions, this is due to the presence of the steam condensation phenomenon and the buoyancy effect. The buoyancy length increases with the rise of velocity for four air fractions, except for the case of velocity of 125 m/s and diameter of 6 mm.
3. A new correlation has been developed for the dimensionless momentum length of jet. The dimensionless momentum length is directly related to Reynolds number and is inversely proportional to Froude number. About 55% of the data points are within the –5% to +5% error band. While the remaining points are within the –20% to +20% error band, with a value for the Pearson product-moment correlation coefficient of $R^2 = 0.941$.
4. A new correlation has been developed for the dimensionless buoyancy length of jet. The dimensionless buoyancy length is directly related to Reynolds number and is inversely proportional to Froude number. More than 45% of the points are within the –5% to +5% error band. While the remaining points are within the –25% to +25% error band with a value for the Pearson product-moment correlation coefficient of $R^2 = 0.835$.

ACKNOWLEDGEMENTS

The authors are indebted to the support of the Spain plan of I+D support to the EXMOTRANSIN project ENE2016-79489-C2-1-P and the Santiago Grisolía Program for its training research personnel.

REFERENCES

[1] Gamble, R.E., Nguyen, T.T., Shiralkar, B.S., Peterson, P.F., Greif, R. & Tabata, H., Pressure suppression pool mixing in passive advanced BWR plants. *Nuclear Engineering and Design*, **204**(1–3), pp. 321–336, 2001. DOI: 10.1016/S0029-5493(00)00363-0.

[2] Kerney, P.J., Faeth, G.M. & Olson, D.R., Penetration characteristics of a submerged steam jet. *AIChE Journal*, **18**(3), pp. 548–553, 1972. DOI: 10.1002/aic.690180314.

[3] Chun, M.-H., Kim, Y.-S. & Park, J.-W., An investigation of direct condensation of steam jet in subcooled water. *International Communications in Heat and Mass Transfer*, **23**(7), pp. 947–958, 1996. DOI: 10.1016/0735-1933(96)00077-2.

[4] Wu, X.-Z., Yan, J.-J., Li, W.-J., Pan, D.-D. & Chong, D.-T., Experimental study on sonic steam jet condensation in quiescent subcooled water. *Chemical Engineering Science*, **64**, pp. 5002–5012, 2009. DOI: 10.1016/j.ces.2009.08.007.

[5] Weimer, J.C., Faeth, G.M. & Olson, D.R., Penetration of vapor jets submerged in subcooled liquids. *AIChE Journal*, **19**(3), pp. 552–558, 1973. DOI: 10.1002/aic.690190321.

[6] Kim, H.Y., Bae, Y.Y., Song, C.H., Park, J.K. & Choi, S.M., Experimental study on stable steam condensation in a quenching tank. *International Journal of Energy Research*, **25**(3), pp. 239–252, 2001. DOI: 10.1002/er.675.

[7] Harby, K., Chiva, S. & Muñoz-Cobo, J.L., An experimental investigation on the characteristics of submerged horizontal gas jets in liquid ambient. *Experimental Thermal Fluid Science*, **53**, pp. 26–39, 2014. DOI: 10.1016/J.EXPTHERMFLUSCI.2013.10.009.

[8] Harby, K., Chiva, S. & Muñoz-Cobo, J.L., Modelling and experimental investigation of horizontal buoyant gas jets injected into stagnant uniform ambient liquid. *International Journal of Multiphase Flow*, **93**, pp. 33–47, 2017. DOI: 10.1016/j.ijmultiphaseflow.2017.03.008.

[9] Chong, D., Zhao, Q., Yuan, F., Wang, W., Chen, W. & Yan, J., Research on the steam jet length with different nozzle structures. *Experimental Thermal Fluid Science*, **64**, pp. 134–141, 2015. DOI: 10.1016/j.expthermflusci.2015.02.015.

[10] Rassame, S., Hibiki, T. & Ishii, M., Void penetration length from air injection through a downward large diameter submerged pipe in water pool. *Annals of Nuclear Energy*, **94**, pp. 832–840, 2015. DOI: 10.1016/j.anucene.2016.04.046.

[11] Igwe, B.U.N., Ramachandran, S. & Fulton, J.C., Jet penetration and liquid splash in submerged gas injection. *Metallurgical Transactions*, **4**(8), pp. 1887–1894, 1973. DOI: 10.1007/BF02665417.

[12] Hoefele, E.O. & Brimacombe, J.K., Flow regimes in submerged gas injection. *Metallurgical Transactions B*, **10**(4), pp. 631–648, 1979. DOI: 10.1007/BF02662566.

[13] Emani, A. & Briens, C., Study of downward gas jets into a liquid. *AlChE Journal*, **54**(9), pp. 2269–2280, 2008. DOI: 10.1002/aic.

[14] Carreau, J.L., Roger, F., Loukarfi, L., Gbahoue, L. & Hobbes, P., Penetration of a horizontal gas jet sumerged in a liquid. *Proceedings of the Intersociety Energy Conversion Engineering Conference*, pp. 315–319, 1986.

[15] Li, W., Meng, Z., Sun, Z., Sun, L. & Wang, C., Investigations on the penetration length of steam-air mixture jets injected horizontally and vertically in quiescent water. *International Journal of Heat and Mass Transfer*, **122**, pp. 89–98, 2018. DOI: 10.1016/j.ijheatmasstransfer.2018.01.075.
[16] Zhou, L., Liu, J., Chong, D. & Yan, J., Numerical analysis on pressure distribution for sonic steam jet condensed into subcooled water. *International Journal of Heat and Mass Transfer*, **99**, pp. 53–64, 2016. DOI: 10.1016/j.ijheatmasstransfer.2016.03.070.
[17] Shukla, S.K., Samad, A.M.N. & Ghosh, S., CFD simulation of steam condensation in a subcooled water pool. *Thermal Science and Engineering Progress*, **2**, pp. 80–86, 2017. DOI: 10.1016/j.tsep.2017.04.006.
[18] Cai, J., Jo, B., Erkan, N. & Okamoto, K., Effect of non-condensable gas on thermal stratification and flow patterns in suppression pool. *Nuclear Engineering and Design*, **300**, pp. 117–126, 2016. DOI: 10.1016/j.nucengdes.2016.01.022.
[19] Song, D., Erkan, N., Jo, B. & Okamoto, K., Dimensional analysis of thermal stratification in a suppression pool. *International Journal of Multiphase Flow*, **66**, pp. 92–100, 2014. DOI: 10.1016/j.ijmultiphaseflow.2014.07.003.